Fracture Mechanics of Concrete Structures
**Proceedings FRAMCOS-3**
AEDIFICATIO Publishers, D-79104 Freiburg, Germany

# FINITE ELEMENT ANALYSIS OF CRACKING DUE TO SHRINKAGE

G.P.A.G. van Zijl
Faculty of Civil Engineering, Delft University of Technology, Delft, The Netherlands

R. de Borst
Faculty of Civil Engineering, Delft University of Technology, Delft, The Netherlands

J.G. Rots
TNO Building and Construction Research, Delft, The Netherlands

## Abstract
In this paper a finite element formulation for the analysis of moisture migration, creep, shrinkage and cracking in cementitious materials, such as masonry, is presented. A decoupled approach is followed, where the pore humidity, the driving force for shrinkage, is solved for from a diffusion equation. The evolution of the shrinkage strain field is then computed and employed in a subsequent mechanical analysis neglecting stress or cracking influence on the pore humidity. The initiation and growth of cracks are simulated in a smeared way by softening, anisotropic Rankine plasticity. Bulk creep is modelled with visco-elasticity, while the other important cause of time-dependence in quasi-static processes, namely the rate-dependence of the bond ruptures leading to fracture, is accounted for by considering the viscosity of the cracking process. The latter contribution is shown to have a regularising effect on the localisation process which accompanies smeared cracking models.
Key words: Pore humidity, shrinkage, creep, anisotropic cracking

## 1 Introduction

Creep and shrinkage in cementitious materials depend strongly on their moisture content. The limited tensile strength and the subsequent softening behaviour of such materials are of equal importance. For realistic analysis of the interaction between shrinkage, creep and

cracking it is imperative to include these phenomena in the formulation, including the so-called Pickett-effect (Pickett 1942). Such a finite element (FE) implementation was reported recently (van Zijl et al. 1998). A decoupled approach was adopted, in which a stress (mechanical) analysis follows the solution of the diffusion equation for the humidity. For the mechanical analysis a smeared cracking approach was followed, employing an orthotropic Rankine plasticity yield criterion.

The above FE model will be outlined briefly in this paper to prepare the ground for discussion of the inclusion of another source of rate-dependence in quasi-static processes into the formulation. While bulk creep, which is modelled with visco-elasticity here, accounts for the stiffness degradation of the entire structural volume in time, the rate-dependence of the breakage of bonds in the fracture zone accounts for the sensitivity to the crack opening velocity. A physical rationale for the latter process and mathematical and algorithmic formulation was given by Wu and Bažant (1993). Here a simplified approach is followed, by considering the viscosity of the fracturing process following Sluys (1992), de Borst et al. (1993) and Wang (1997). This approach is appealing, because the rate term is retained explicitly, ensuring visco-plastic regularisation of the conventional smeared-crack approach.

Finally, a case study is presented in which a based-restrained shrinking masonry wall is analysed with and without the crack opening rate-dependence.

## 2 Modelling creep and shrinkage

Shrinkage depends directly on the pore pressure (Bažant 1988), which is most commonly obtained from the nonlinear diffusion equation:

$$\dot{h} = \nabla \bullet [D(h)\, \nabla h] \tag{1}$$

where

$h = p/p_s$ is the relative pore humidity, which is the pore pressure relative to the pore pressure at saturation and
$D(h)$ is the diffusivity, accounting for all diffusion mechanisms.

The boundary conditions can be

*essential*, i.e. fixed humidity: $h_s = h_e$
*natural*, i.e. fixed flux: $q_s$
*convective* boundary: $q_s = \beta\,(h_s - h_e)$

where subscript $_s$ indicates the value at the boundary, or surface, $h_e$ is the environmental humidity and $\beta$ is the surface convection coefficient.

For a finite increment in time $\Delta t$, the following shrinkage-pore pressure relation has been proposed:

$$\Delta \varepsilon^s = \alpha^o_{sh}\, \Delta h \tag{2}$$

with
$$\alpha_{sh}^{o} = \begin{cases} \text{constant} & 0.4 \leq h \leq 1.0 \\ 3\varepsilon^{s,\infty}\left[(h^t)^2 - \left(h^{t+\Delta t}\right)^2\right] & h \leq 0.99 \end{cases} \tag{3}$$

by Wittmann (1977) and Bažant (1988) respectively. $\varepsilon^{s,\infty}$ scales the shrinkage to the maximum expected shrinkage strain.

It is accepted that viscous behaviour can be ascribed to moisture migration, but no direct way of determining creep characteristics exists. Here visco-elasticity is employed to capture the bulk creep. By inclusion of the superposition and proportionality principles, the creep is expressed by the stress relaxation formulation:

$$\boldsymbol{\sigma} = \int_0^t R(t,\tau)\boldsymbol{D}\dot{\boldsymbol{\varepsilon}}\,\mathrm{d}\tau. \tag{4}$$

$R(t,\tau)$ is the relaxation modulus which reflects the (visco-elastic) stress at time t that is caused by a unit strain acting since time $\tau$ and $\boldsymbol{D}^{-1}$ is the matrix representation of the fourth order tensor

$$D_{ijkl} = \frac{1}{2}(1-\nu)(\delta_{ik}\delta_{jl} + \delta_{il}\delta_{jk}) - \nu\delta_{ij}\delta_{kl}. \tag{5}$$

For computational convenience equation (4) is recast into differential, rate-type equations. This entails a degeneration of the kernel $R(t,\tau)$ into sums and products of functions of single time variables:

$$R(t,\tau) \;=\; E_0(\tau) + \sum_{\alpha=1}^{N} E_\alpha(\tau)\exp\left(-\frac{t-\tau}{\lambda_\alpha}\right). \tag{6}$$

Equation (6) can be represented rheologically by a Maxwell chain, as shown in the visco-elasticity part of Fig. 1. $E_\alpha$ is the elasticity modulus, $\lambda_\alpha = \eta_\alpha/E_\alpha$ the relaxation time and $\eta_\alpha$ the viscosity of chain element $\alpha$.

Considering the time interval $\Delta t$ with the associated increments of stress and strain

$$\Delta\boldsymbol{\sigma} \;=\; {}^{t+\Delta t}\boldsymbol{\sigma} - {}^{t}\boldsymbol{\sigma} \tag{7}$$

$$\Delta\boldsymbol{\varepsilon} \;=\; {}^{t+\Delta t}\boldsymbol{\varepsilon} - {}^{t}\boldsymbol{\varepsilon} \tag{8}$$

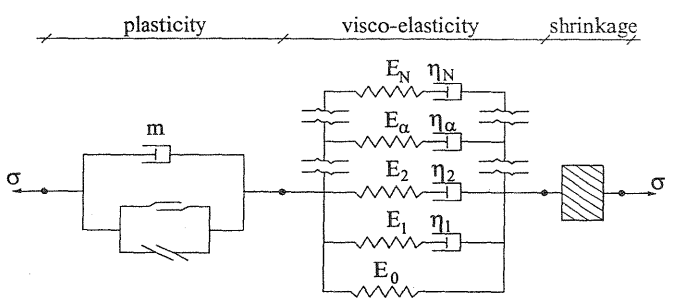


Fig. 1. Maxwell chain coupled in series with plastic flow and shrinkage strain elements.

the stress increment can be expressed as

$$\Delta\boldsymbol{\sigma} = \boldsymbol{D}^{ve}\Delta\boldsymbol{\varepsilon} + {}^{t}\tilde{\boldsymbol{\sigma}} \tag{9}$$

where

$$\boldsymbol{D}^{ve} = \tilde{E}(t^*)\boldsymbol{D} \tag{10}$$

$$\tilde{E}(t^*) = E_0(t^*) + \sum_{\alpha=1}^{N} \frac{E_\alpha(t^*)}{\Delta t/\lambda_\alpha}\left[1 - e^{-\Delta t/\lambda_\alpha}\right] \tag{11}$$

$${}^{t}\tilde{\boldsymbol{\sigma}} = -\sum_{\alpha=1}^{N}\left[1 - e^{-\Delta t/\lambda_\alpha}\right]{}^{t}\boldsymbol{\sigma}^{\alpha} \tag{12}$$

$${}^{t}\boldsymbol{\sigma}^{\alpha} = \int_0^t E_\alpha(\tau)\,\exp\left(-\frac{t-\tau}{\lambda_\alpha}\right)\boldsymbol{D}\dot{\boldsymbol{\varepsilon}}\,\mathrm{d}\tau. \tag{13}$$

In case of an aging material, $E_\alpha(\tau)$ is evaluated at $t^*$, with $t \le t^* \le t + \Delta t$.

The internal variables given by equation (13) are the stresses in the Maxwell elements at the end of the previous time step ($t$). Using equation (7) in combination with (9)-(13) the total current stress can be written as

$${}^{t+\Delta t}\boldsymbol{\sigma} = {}^{t}\boldsymbol{\sigma} + \boldsymbol{D}^{ve}\Delta\boldsymbol{\varepsilon} + {}^{t}\tilde{\boldsymbol{\sigma}}. \tag{14}$$

A plasticity-based crack model is adopted. Assuming the creep and shrinkage strains to be additive to the plastic strain, (Fig. 1) equation (14) can be expanded as:

$${}^{t+\Delta t}\boldsymbol{\sigma} = {}^{t}\boldsymbol{\sigma} + \boldsymbol{D}^{ve}\left(\Delta\boldsymbol{\varepsilon} - \Delta\boldsymbol{\varepsilon}^{s} - \Delta\boldsymbol{\varepsilon}^{p}\right) + {}^{t}\tilde{\boldsymbol{\sigma}} \tag{15}$$

where the plastic strain increment follows from a non-associative plastic flow rule

$$\Delta\boldsymbol{\varepsilon}^{p} = \Delta\lambda\frac{\partial g}{\partial\boldsymbol{\sigma}}. \tag{16}$$

The creep dependence on the humidity can be expressed in terms of stress-dependent shrinkage (Bažant 1988, van Zijl et al. 1998) as:

$$\Delta\boldsymbol{\varepsilon}^{s} = \alpha_{sh}^{o}\Delta h\left(\boldsymbol{P} + \boldsymbol{r}\boldsymbol{\sigma}\right) = \Delta\varepsilon^{o,s}\left(\boldsymbol{P} + \boldsymbol{r}\boldsymbol{\sigma}\right) \tag{17}$$

with, for a plane stress state

$$\boldsymbol{P} = \{\ 1\ 1\ 0\ \}^{\mathrm{T}} \tag{18}$$

$$\boldsymbol{r} = \mathrm{diag}[\ r_x\ r_y\ 0\ ] \tag{19}$$

$r_x$ and $r_y$ being material parameters in the range $\frac{0.1}{f_t} \le r_i \le \frac{0.6}{f_t}$ (Bažant 1988). Obviously, the general case that $r_x \neq r_y$ would represent an anisotropic character of stress-induced shrinkage.

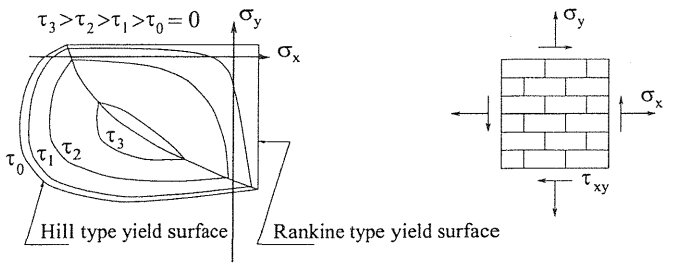


Fig. 2. Plasticity based material model (Lourenço 1996).

To account for the different strengths parallel and perpendicular to bed joints in masonry, an anisotropic version of the Rankine yield criterion is employed, combined with a Hill criterion under compressive loadings (Fig. 2).

In the analyses reported here only the tension criterion is activated. The degradation process is governed by different values of the tensile strength ($f_{tx}$, $f_{ty}$) and the fracture energy ($G_{ftx}$, $G_{fty}$) along each material axis. The shape of the Rankine yield function is determined by a parameter $\alpha$, which controls the shear stress contribution to tensile failure, $\alpha = 1.0$ being the standard Rankine value.

## 3 Rate-dependent crack growth

The time-dependence of fracture is caused not only by the creep in the bulk of the material, but also the rate-dependence of the breakage of bonds in the fracture process zone. This contribution has been shown to have a stabilising influence in dynamic problems (Sluys 1992, Wang 1997), as well as quasi-static problems (de Borst et al. 1993, Wang 1997). The loss of hyperbolicity and ellipticity in dynamic and quasi-static problems respectively and the ensuing mesh dependence during the formation and growth of cracks are avoided.

Departing from the Maxwell-Boltzmann distribution of frequency at which the energy of thermally vibrating atoms exceeds the level at which the bonds rupture, the so-called activation energy, the following expression for the crack opening rate $\dot{w}$ can be derived (Wu and Bažant 1993):

$$\dot{w} = \dot{w}_r \sinh\left[\frac{\sigma - \bar{\sigma}(w)}{k\ (\bar{\sigma}(w) - k_0\ f_t)}\right] e^{\frac{Q}{RT_0} - \frac{Q}{RT}} \tag{20}$$

where $\dot{w}_r$ is a constant, reference opening velocity, $\bar{\sigma}(w)$ describes the strength degradation with crack opening displacement, $Q$ is the activation energy, $R$ the gas constant, $T$ the temperature and $T_0$ the reference temperature. The material parameter $k$ is estimated to be in the range 0.01 - 0.08 from the knowledge that for a $10^4$-fold increase of the loading rate a 25% increase in peak strength is

found experimentally. The material parameter $k_0$ is an offset factor to prevent the denominator in equation (20) from becoming zero. For isothermal conditions and by approximating the crack opening displacement $w = l_b\,\kappa$, with $l_b$ the crack band width and $\kappa$ the crack strain equation (20) can be rewritten as

$$\sigma = \bar{\sigma}(\kappa)\left[1 + k\,\sinh^{-1}\left(\frac{\dot{\kappa}}{\dot{\kappa}_r}\right)\right] + k\,k_0\,f_t\,\sinh^{-1}\left(\frac{\dot{\kappa}}{\dot{\kappa}_r}\right). \tag{21}$$

Here an alternative approach is followed. As illustrated in Fig. 1 crack rate-dependence is captured via a dashpot of viscosity $m$ parallel to the plasticity elements. The rate-dependent cracking stress is

$$\sigma = \bar{\sigma}(\kappa)\left[1 + \frac{m}{f_t}\,\dot{\kappa}\right]. \tag{22}$$

For the Rankine formulation employed here $\kappa = \varepsilon_1^p$, the principal plastic strain. Exponential softening of the tensile strength is assumed:

$$\bar{\sigma}(\kappa) = f_t\,e^{-\frac{f_t\,l_b}{G_f}\kappa}. \tag{23}$$

As an illustration of the visco-plastic regularisation the one-dimensional tension bar shown in Fig. 3a was analysed. The bar has a linear increasing cross section A such that A(L)/A(0) = 1.2 to avoid a homogeneous solution. It is discretised into 10, 20 and 40 elements along the length respectively. Fig. 3b shows the mesh-dependent energy dissipation and Fig. 3c,d the mesh-dependent localisation zone width if the rate term is neglected (m=0). For $m \geq 1$ N s/mm$^2$ energy dissipation and localisation can be seen to be mesh-objective. Note that the divergence in stress-displacement response for the different meshes after some degradation (for the case of $m = 1$ N s/mm$^2$ after 0.2 mm displacement) is caused by the exponentially diminishing rate term contribution (equations (22,23)). This manifests as eventual localisation in the first element as is seen in Fig. 3d for $m = 1$ N s/mm$^2$ and to a lesser extent for $m = 2$ N s/mm$^2$. A possible remedy is to include a rate-dependent residual term, such as the last term in equation (21).

## 4 Case study

Restrained shrinkage cracking of masonry walls is one of the major causes of damage to buildings in the Netherlands. Nevertheless, movement joint design remains an art, guided by rules of thumb. To gain insight in wall behaviour and as an initial step towards deriving rational design rules, a base-restrained shrinkage masonry wall was analysed. The single leaf wall adopted in earlier studies by Rots et al.

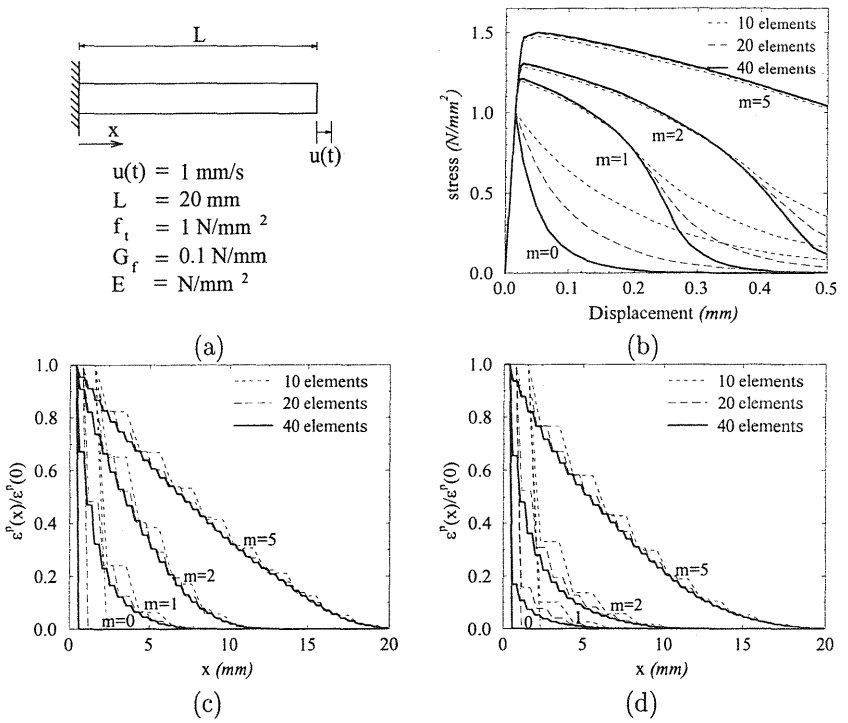


Fig. 3. Tension bar showing (b) stress in the bar at the constraint, (c,d) plastic strain along the bar at 0.21 mm and 0.41 mm displacement respectively.

(1994) was chosen for this study. It is shown schematically in Fig. 4 with a typical crack pattern. Apart from its own weight an in-plane bearing load of eight times own weight was assumed.

### 4.1 Diffusion analysis

Despite the discrete nature of masonry a continuum approach was followed for the diffusion analysis. A two-dimensional analysis of the wall plane was performed, with the simplifying assumption of no flux through the base interface. A plane of interface elements on both the inner and outer face of the wall and boundary elements at the three remaining edges accounted for interaction with the environment. Surface convection was prescribed with a coefficient $\beta = 5.0$ mm/day and $h_e = 0.6$. A diffusivity coefficient $D(h) = 0.22e^{5.4h}$, was employed. These parameter values are close to those found for concrete (Alvaredo 1994), in the absence of experimental data for masonry.

With an assumed uniform initial pore humidity, a uniform humidity evolution is found. This is not surprising because of the large surface which is exposed to the environment. Only by accounting for the

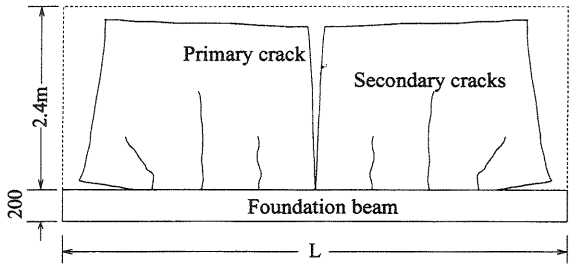


Fig. 4. Observed crack pattern in base-restrained shrinkage wall.

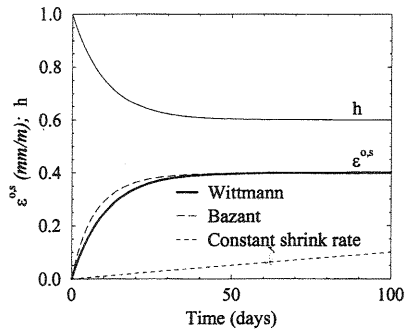


Fig. 5. Humidity (h) and free shrinkage strain ($\varepsilon^{o,s}$) in the wall.

random nature of material properties and nonuniform environmental conditions, nonuniform pore humidity can be found by a diffusion analysis of such a wall. The humidity variation in time is shown in Fig. 5, along with the free shrinkage strain obtained from equation (3) with $\alpha^o_{sh} = 0.001$.

## 4.2 Mechanical analysis

Only a half of the wall was modelled, because of symmetry. Four-noded plane-stress quadrilateral elements were employed. Material parameters typical for calcium silicate masonry were chosen (see Table 1). Tensile strengths and fracture energies that are 10% higher than tabulated were employed for the wall away from the primary crack to simulate material property variation in a simple way and to avoid possible bifurcations.

The stiff foundation beam was assumed not to shrink. Interface

Table 1. Masonry wall material parameters employed.

| Young's modulus | Poisson's ratio | Tensile strength | | Fracture energy | | |
|---|---|---|---|---|---|---|
| E $N/mm^2$ | $\nu$ | $f_{tx}$ $N/mm^2$ | $f_{ty}$ $N/mm^2$ | $G_{ftx}$ $N/mm$ | $G_{fty}$ $N/mm$ | $\alpha$ |
| 5000 | 0.2 | 0.4 | 0.3 | 0.04 | 0.02 | 1.0 |

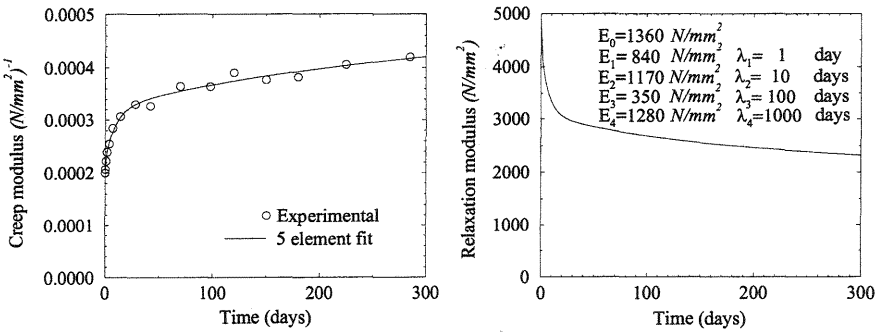


(a) (b)

Fig. 6. (a) Measured creep and fitted five-element Dirichlet function. (b) Relaxation function derived from (a).

elements were employed to account for shearing and debonding along the base-wall interface. A Coulomb cohesive-friction model with cohesion $0.6N/mm^2$ softening exponentially to zero, a fracture energy $0.1N/mm$ and a friction angle $37^o$ was adopted. A limited tensile strength $0.3N/mm^2$ was degraded to zero exponentially with a fracture energy $0.02N/mm$. The cohesive-friction model and the tension cut-off were incorporated in a multi-surface plasticity formulation (Lourenço 1996).

Because of lack of tensile creep measurements, a typical compressive creep behaviour of calcium silicate masonry (van der Pluijm & Wubs 1996) was employed for the least-squares fitting of a five-element Kelvin-Voigt chain (see Fig. 6a). For the same reason aging was not considered, despite evidence of masonry compressive creep aging (Shrive et al. 1997). By constant strain analysis the five-element Maxwell chain shown in Fig. 6b was derived.

For the initial analyses stress dependence of the shrinkage was not included. Also, no rate term was included (m=0). Instead, a crack band width ($l_b$) related to the area of an element (Lourenço 1996) was assumed to strive at mesh-objective energy dissipation. The crack patterns and the maximum crack width development with free shrinkage obtained from the diffusion analysis with a constant shrinkage coefficient (Wittmann 1977) are shown in Fig. 7. The primary crack initiates near the base and grows upward. The analysis was terminated just before the point of snap-through. In time-dependent analyses by van Zijl & Rots (1997) an arc-length method was successfully employed to trace the snap-through. In the present time-dependent analysis a special arc-length scheme (van den Boogaard et al. 1994) should be employed. However, the snap-back physically means that inertia, ignored in this quasi-static analysis, becomes important as the wall separates dynamically along the primary crack.

To illustrate the rate-dependence, the analysis was repeated for

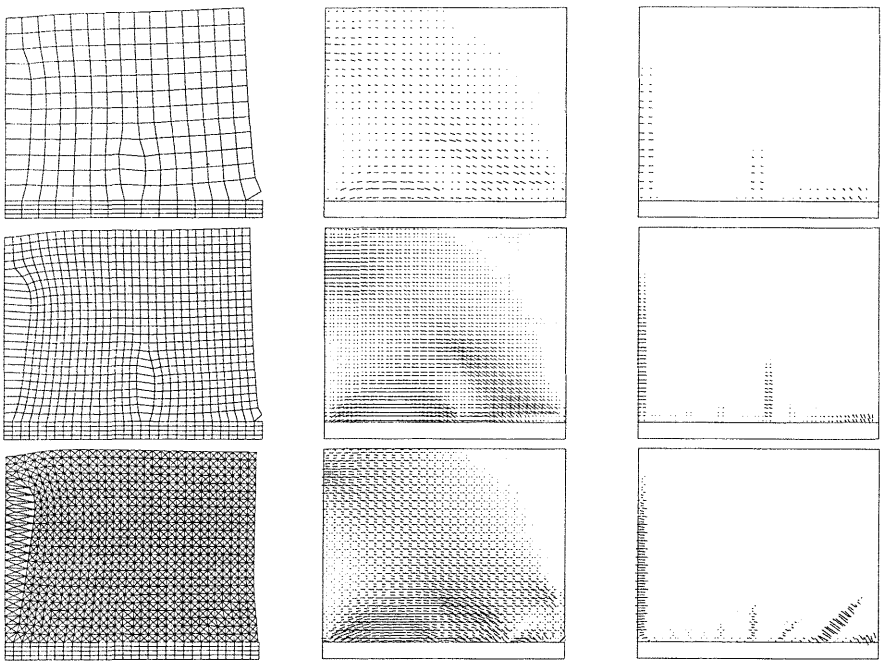


(a) Mesh-dependent crack pattern.

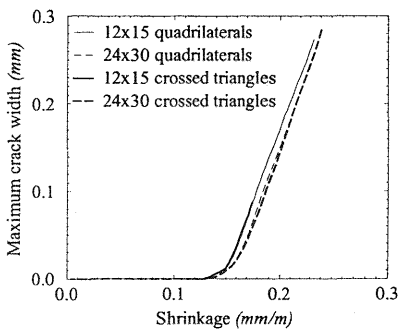


(b) Primary crack width.

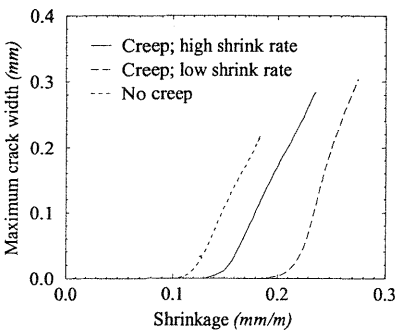


(c) Primary crack width for different shrinkage rates.

Fig. 7. Base-restrained shrinking masonry wall response.

the lower, constant shrinkage rate shown in Fig. 5. Obviously, we now obtain a smaller maximum crack width for the same amount of shrinkage. Conversely, a higher maximum crack width is computed when imposing a very high shrinkage rate. The limiting case of an infinite shrinkage rate has been simulated by an analysis in which creep was set to zero (Fig. 7c).

Mesh objectivity regarding element size and shape was also investigated (see Fig. 7a,b). Different crack patterns are found, with per-

sistent vertical secondary cracking when employing quadrilateral elements, as opposed to a $45^o$ secondary crack obtained with the crossed triangular mesh. However, no significant difference in primary crack width is found. For a different choice of material parameters the non-objectivity regarding crack spacing and alignment might have significant influence on global behaviour, as shown in Fig. 8. Here only a 5% difference in strength and fracture energies between the primary crack region and the rest of the wall was prescribed. Now the secondary crack becomes dominant in the quadrilateral mesh, as can be seen from the arrest of the primary crack at a width of 0.1 mm when the shrinkage strain exceeds 0.2 mm/m (Fig. 8b).

By inclusion of a rate term as outlined in section 3 the crack patterns shown in Fig. 9 are obtained. The primary crack evolution as well as the secondary crack location and orientation are now captured properly. A dashpot with high viscosity ($m = 1000$ - $m = 2000$ N day/mm$^2$, the response for the latter shown) is needed to achieve

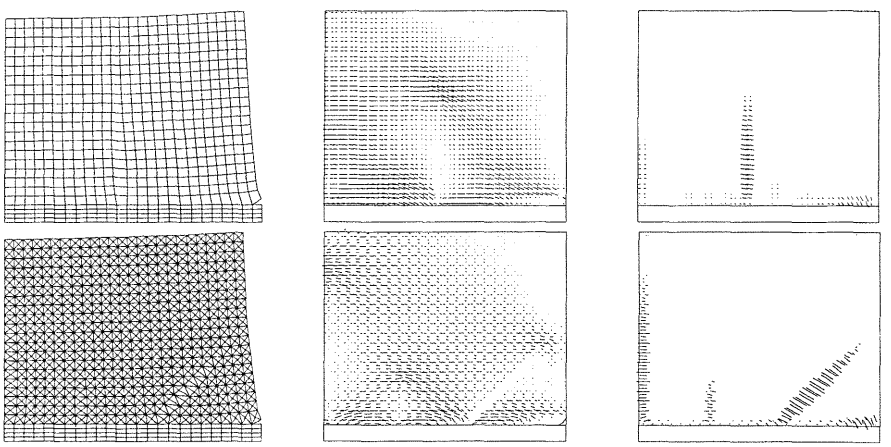


(a) Mesh-dependent crack pattern.

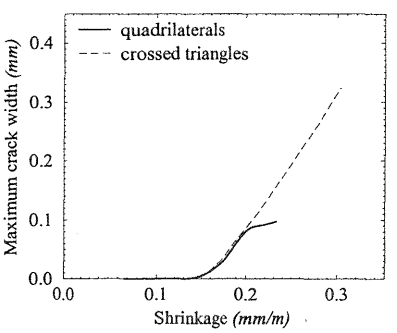


(b) Mesh-dependent primary crack width.

Fig. 8. Mesh sensitivity study.

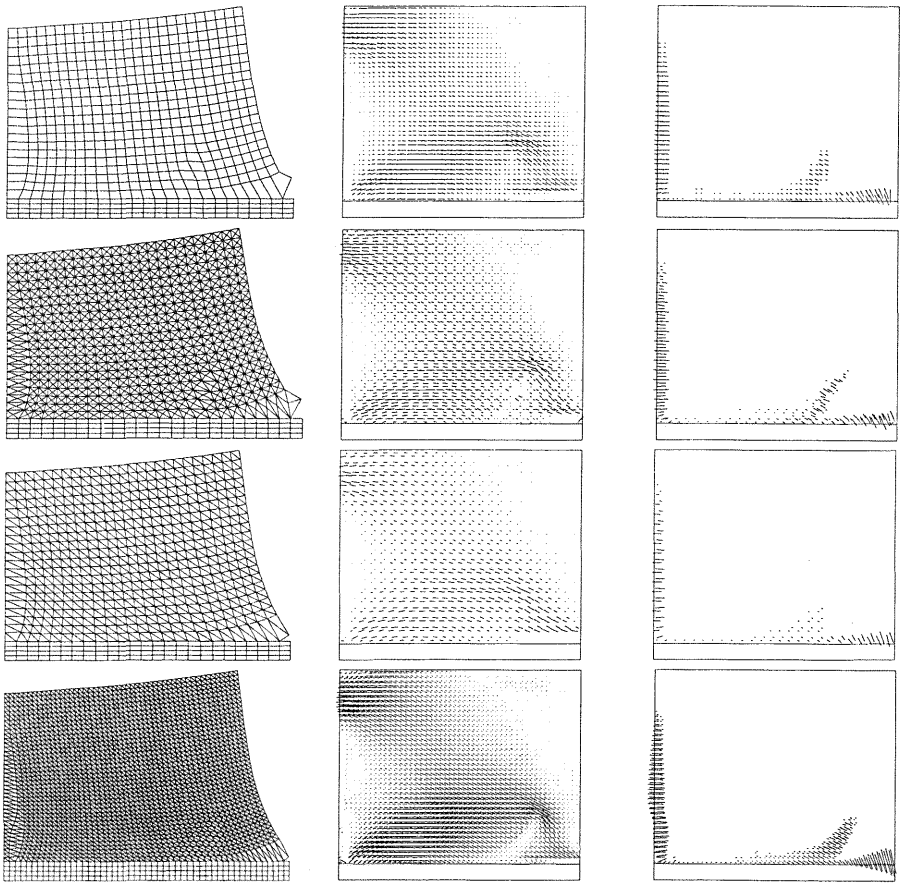


(a) Mesh-independent crack pattern.

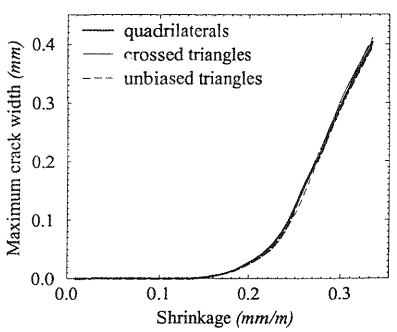


(b) Primary crack width.

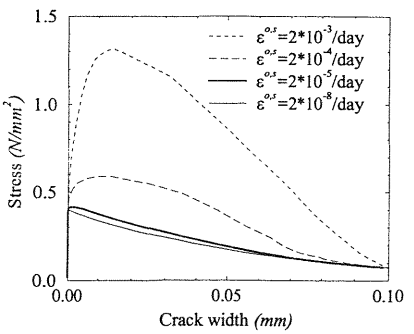


(c) Mechanical response at various shrinkage rates.

Fig. 9. Crack pattern and spacing objectivity when including the crack growth rate term.

this regularisation. Note that this viscosity is in the order of that of the visco-elastic chain element with the shortest relaxation time. One should keep in mind that the shrinkage is such a slow process - $\varepsilon^{o,s} \approx 2 \times 10^{-5}$/day during the first 10 days - that it requires a high viscosity to modify the mechanical response, as shown for different loading rates in Fig. 9(c). In the figure it can be seen that an increase of about 50% in peak strength is achieved by $10^4$-fold increase in the shrinkage rate (25% for $m = 1000$ N day/mm$^2$), but that there is an excessive strength increase beyond this loading range ($\varepsilon^{o,s} > 2 \times 10^{-4}$/day). To generalise the current formulation for application in loading ranges beyond the current loading range a logarithmic-type formulation such as equation (21) should be considered, but with preservation of the rate term to retain the regularisation ability.

## 5 Conclusions

A formulation has been presented of the interaction between moisture migration, shrinkage, creep and cracking of cementitious materials. A simple extension of standard plasticity equations to incorporate visco-elasticity has been elaborated. Anisotropic cracking has been captured by prescribing the significant differences in strength in orthogonal directions.

Crack patterns were found to be in agreement with observations in buildings when analysing base-restrained shrinking masonry walls. A maximum primary crack width was found, which is objective with regard to FE size and type, but the position and orientation of the secondary cracking appeared to be mesh dependent. By inclusion of a stress-dependence of the crack opening velocity a mesh objective prediction of secondary cracking was obtained.

## 6 Acknowledgments

This research is supported by the Netherlands Technology Foundation STW, applied science division of NWO under grant DCT 44.3406, and by CUR committee A33. The model described here was implemented into a pilot version of the DIANA finite element package, which was subsequently employed for the calculations.

## 7 References

Alvaredo, A.M. (1994) **Drying shrinkage and crack formation.** Building materials reports No 5, ETH Laboratory for building materials, Zürich, Switzerland.

Bažant, Z.P., Ed. (1988) **Mathematical modelling of creep and shrinkage of concrete.** John Wiley & Sons.

de Borst, R., van den Boogaard , A.H., Sluys, L.J. and van den Bogert, P.A.J. (1993) Computational issues in time-dependent

deformation and fracture of concrete, in **Creep and Shrinkage of Concrete** (eds. Z.P. Bažant and I. Carol), E.&F.N.Spon, London, 309-326.

Lourenço, P.B. (1996) **Computational strategies for masonry structures**. Dissertation, Delft Univ. of Tech., Delft, The Netherlands.

Pickett, G. (1942) The effect of change in moisture content on the creep of concrete under a sustained load. **Journal of the ACI**, 38,333-355.

Rots, J.G., Berkers, W.G.J. and van den Heuvel, H.A.J.G. (1994) Towards fracture mechanics based design rules for movement-joint spacing, in **Proc. 10th Int. Brick/Block Masonry Conf.** (eds. N.G. Shrive and A. Huizer), Univ. of Calgary, Canada, 2,707-718.

Shrive, N.G., Sayed-Ahmed, E.Y. and Tilleman, D. (1997) Creep analysis of clay masonry assemblages. **Canadian J. of Civil Eng.**, 24(3),367-379.

Sluys, L.A. (1992) **Wave propagation, localization and dispersion in softening solids**. Dissertation, Delft Univ. of Tech., Delft, The Netherlands.

van den Boogaard, A.H., de Borst, R. and van den Bogert, P.A.J. (1994) An adaptive time-stepping algorithm for quasistatic processes. **Comm. Num. Meth. in Eng.**, 10,837-844.

van der Pluijm, R. and Wubs, A.J. (1996) **Het Tijdsafhankelijk vervormingsgedrag van Metselwerk**. Report 96-CON-R0901-02, TNO-Bouw, Delft, The Netherlands.

van Zijl, G.P.A.G. and Rots, J.G. (1997) Towards numerical prediction of structural masonry behaviour, to be published in **Proc. 4th Int. Symp. on Comp. Meth. in Struct. Masonry** (eds. J. Middleton & G.N. Pande), Pineridge Press, Swansea, UK.

van Zijl, G.P.A.G., de Borst, R. and Rots, J.G. (1998) FE analysis of the interaction between moisture migration, creep, shrinkage and cracking, to be published in **Computational modelling of concrete structures EURO-C 1998** (eds. H. Mang, N. Bićanić and R. de Borst).

Wang, W.M. 1997. **Stationary and propagative instabilities in metals - a computational point of view**. Dissertation, Delft Univ. of Tech., Delft, The Netherlands.

Wittmann, F.H. (1977) Grundlagen eines Modells zur Beschreibung charakteristischer Eigenschaften des Betons. **Schriftenreihe Deutscher Ausschuss für Stahlbeton**, Heft 290, Berlin, 43-101.

Wu, Z.S. and Bažant, Z.P. (1993) Finite element modelling of rate effect in concrete fracture with influence of creep, in **Creep and Shrinkage of Concrete** (eds. Z.P. Bažant and I. Carol), E.&F.N.Spon, London, 427-432.